Optics Letters

All-solid-state multipass spectral broadening to sub-20 fs

Kilian Fritsch,[1,*] Markus Poetzlberger,[2] Vladimir Pervak,[1] Jonathan Brons,[1] and Oleg Pronin[2]

[1]Ludwig-Maximilians-Universität München, Am Coulombwall 1, D-85748 Garching, Germany
[2]Max-Planck-Institut für Quantenoptik, Hans-Kopfermann-Str. 1, D-85748 Garching, Germany
*Corresponding author: kilian.fritsch@physik.uni-muenchen.de

Received 30 May 2018; revised 14 July 2018; accepted 16 July 2018; posted 27 August 2018 (Doc. ID 332948); published 20 September 2018

In this work, we present a nonlinear spectral broadening and compression scheme based on self-phase modulation in bulk media inside a Herriott-type multipass cell. With this reliable approach, we achieved a spectral broadening factor of 22 while maintaining an efficiency of over 60% at an average input power of 100 W, and an excellent output beam quality with $M^2 = 1.2$. The output pulses were compressed to 18 fs, with the broadest spectrum supporting a Fourier-transform limit of 10 fs. The high efficiency and approximately four-optical-cycle pulse duration mark an important milestone towards the realization of a compact, high power oscillator-based driver for XUV frequency combs and other nonlinear processes.

OCIS codes: (140.7090) Ultrafast lasers; (190.7110) Ultrafast nonlinear optics; (320.5520) Pulse compression; (140.3580) Lasers, solid-state.

https://doi.org/10.1364/OL.43.004643

Numerous spectroscopic applications in the deep-UV and extreme-UV (XUV) spectral ranges would greatly benefit from a stable laser source emitting in those ranges. One such application is the spectroscopy of the 1S–2S transition of He^+-ions, which requires coherent radiation near 60.8 nm to drive this two-photon transition [1], and constitutes a milestone yet to be reached. Next-generation ultraprecise Th-based atomic clocks represent another application requiring deep-UV sources in the 67–96 nm region [2]. One way to reach these wavelengths is through high harmonic generation (HHG) in, for example, noble gases. To efficiently drive the XUV generation process, pulse durations below 20 fs are advantageous [3,4]. However, even in this case, only efficiencies of about 10^{-6} can be reached. To compensate for this low efficiency, the use of a driver with high average power is necessary. The intensity noise of the laser driver is potentially a major obstacle towards high-precision spectroscopy applications because significant noise multiplication is expected during the conversion to the XUV [5]. The high-frequency (>100 kHz) component can be especially difficult to compensate for. Moreover, this intensity noise is usually highly correlated with the noise of the carrier-envelope offset (CEO) frequency. CEO stabilization is thus one of the main prerequisites for high-precision spectroscopy applications. This requirement can be satisfied using bulk solid-state oscillators, which have excellent intensity-noise properties in the high-frequency range >100 kHz [6]. In particular, high power thin-disk (TD) oscillators exhibiting shot-noise limited performance (>100 kHz) [7], in tandem with external spectral broadening (SB) and compression, may proof themselves as excellent compact HHG drivers.

Unfortunately, SB techniques based on fibers are prone to damage and sensitive to alignment, especially combining high average (>50 W) and high peak power (>10 MW). Moreover, high repetition rate sources (>20 MHz) in conjunction with gas-filled hollow-core fibers can cause steady-state plasma formation, which in turn can degrade the stability of the setup [8,9]. Similar problems might arise with the multiple-plate approach demonstrated by Lu *et al.* [10] which relies on strong self-focusing and slight ionization in the plates. SB techniques in bulk materials [11–13] or in gas-filled multipass cells [14,15] promise to be peak-power scalable beyond the levels provided by gas-filled capillaries. However, until recently, reported bulk-based SB techniques were limited in efficiency, beam quality, and bandwidth.

In this Letter, we show a highly adaptable laser-system based on TD and bulk-SB providing outputs with pulse durations of 84, 43, and 16 fs. High passive stability and robust operation of the laser system is observed. The all-bulk setup is highly efficient and provides a SB factor of 22—to our knowledge the highest factor reported using such schemes. The SB factor is calculated by taking a ratio of the spectrum's Fourier transform limit (FTL) at the input and output of the spectral broadening arrangement. The compressed pulses are more than a factor of two shorter than reported in earlier publications [16–18].

Upon propagation through materials with cubic (χ^3) nonlinearity, an intense laser pulse will experience self-phase modulation (SPM), which introduces new frequencies. However, self-focusing can strongly deform the spatial Gaussian profile and thereby reduce the achievable peak intensities by decreasing the beam quality (M^2 factor) and throughput efficiency [19,20]. Additionally, the Gaussian spatial intensity profile in bulk material leads to different temporal intensity-slopes at different radial positions of the beam which results in spatial inhomogeneity. In comparison, the spatially distributed spectral components in fibers are homogeneous across the whole beam

due to the continuous spatial mixing within the propagating waveguide-mode and simultaneous SB due to SPM [21]. A waveguide-like periodic structure consisting of focusing elements, nonlinear media, and free space can mimic similar behavior [16–18]. For multipass geometries, transmission efficiencies of over 90% were demonstrated with an increased bandwidth that should allow compression by a factor of up to six [16]. The main prerequisite for such a high throughput efficiency is a low peak nonlinear phase-shift per pass (φ) through the nonlinear medium. Qualitative numerical simulations (detailed methods in [22,23]) show that the expected beam quality M^2 after the bulk SB strongly depends on φ [Fig. 1(a)]. The simulations provide the rotationally symmetric spectral intensity distribution $S(N, r, \omega)$ at a certain plane in the multipass system, which consists of repeating focusing mirrors with radius of curvature (ROC) of 500 mm and a separation distance of 894 mm, and a 6.35 mm thick fused-silica (FS) plate placed between the mirrors. The parameters N, r, ω denote the number of roundtrips, the radial distance from the optical axis, and the angular frequency, respectively. This facilitates the computation of the full width at half-maximum (FWHM) duration of the transform limited pulse $\tau(N, r)$. To quantify the spectral-spatial homogeneity, we define $\sigma(N) = \frac{\sigma'}{\mu}$ with the standard deviation $\sigma' = \sqrt{n^{-1} \sum_{r'=0}^{r'=r} (\tau(N, r')E(r') - \mu)^2}$ and the mean value $\mu(N) = n^{-1} \sum_{r'=0}^{r'=r} \tau(N, r')E(r')$ with the number of radial grid points n and energy normalization $\int_0^\infty E(r')\mathrm{d}r' = 1$. Figure 1(b) (top) shows that σ stays small, i.e., the beam remains homogeneous, if φ stays below 0.6. $\sigma(N)$ increases at larger φ, and the beam quality quickly deteriorates. The simulation shows an approximately linear increase in relative bandwidth [Fig. 1(b), bottom] beyond five passes, in full agreement with the behavior predicted analytically [24]. The focusability of the entire beam in the experiment, which is used here as a metric for the efficiency of the SB process, is quantified by the M^2 parameter. It increases for nonlinear phase-shifts above 0.6 [Fig. 1(a)] in the given configuration. If φ is kept below this threshold, the beam profile does not deteriorate, and continued propagation still results in a homogeneous spectral distribution [Fig. 1(b), top]. Recently, Weitenberg *et al.* [17] studied the output beam-homogeneity of such multipass systems experimentally and proved it to be excellent for low nonlinear phase-shifts per pass. A large number of passes

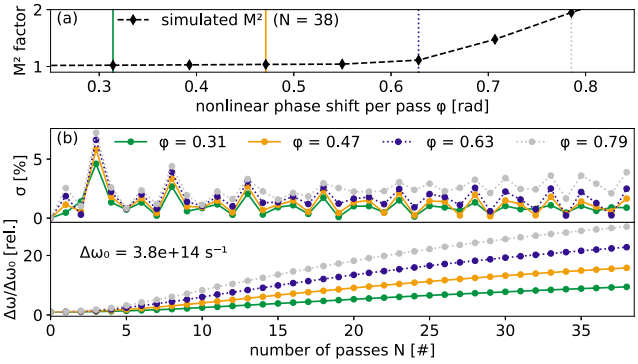

Fig. 1. (a) Simulated beam quality factor M^2 for all-solid-state multipass SB. (b) (Top): Simulated evolution of σ over 38 roundtrips for different φ. For φ over 0.6 the homogeneity degrades. (Bottom): Simulated relative bandwidth over 38 roundtrips for different φ.

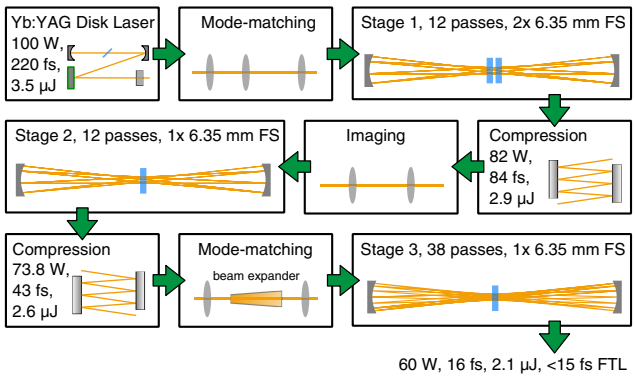

Fig. 2. Schematic setup for the nonlinear pulse compression.

through the nonlinear medium is thus necessary for strong and efficient SB.

The Herriott cell (HC) [25] is a simple multipass geometry consisting of two concave mirrors facing each other on a common optical axis. An off-axis injected beam can traverse back and forth on the cell mirrors forming an elliptical pattern. Beam injection and extraction are realized in this work by a small scraper mirror in front of one of the cell mirrors. Incoming and outgoing beams are angularly separated. The number of passes is determined by the ratio of the beam diameter on the mirror surface to the mirror size. As opposed to other types of multipass cells, e.g., the white cell [26], the foci generated by a HC, when mode-matched properly, lie in the symmetry plane of the arrangement. For the SB setup, this enables the use of a single, large-aperture broadening medium allowing tens of passes with a compact footprint. The HCs in this work fullfil the re-entrant condition and are thus imaging the in- and output-planes [27], hence they preserve the beam stability. A scheme of the entire experimental setup is depicted in Fig. 2(b), and a survey of its parameters is given in Table 1. The driving laser is a Kerr-lens mode-locked TD Yb:YAG oscillator similar to [9] emitting over 100 W of average power at a repetition rate of 28.3 MHz and a FWHM pulse duration of 220 fs, resulting in 14 MW of peak power. Three HCs (Fig. 3) serve as the SB setup. This provides flexibility with regard to the pulse compression factor, and also enables study of the influence of the nonlinear phase-shift on the temporal pulse quality such as pedestals and satellite pulses. The three SB stages each comprise an antireflection (AR) coated FS substrate in the center of the HCs and curved dispersive mirrors designed to balance the second- and third-order material dispersion of the broadening medium by −120 fs^2

Table 1. Experimental Performance of the Broadening Setup; Compressed FWHM Pulse Duration τ_{FWHM}, Per-Stage Efficiency η, Average Power P_{avg}, Peak Power P_{peak}, Fourier Transform Limited Pulse Duration and Maximum Achievable Peak Power in Parenthesis

	τ_{FWHM} [fs]		η [%]	P_{avg} [W]	P_{peak} [MW]	
Oscillator	220	(220)	—	100	14	—
1st stage	84	(75)	82	82	26	(28)
2nd stage	43	(42)	90	74	49	(54)
3rd stage air	18	(18)	81	60	50	(98)
3rd stage vac	16	(14)	82	60	60	(116)

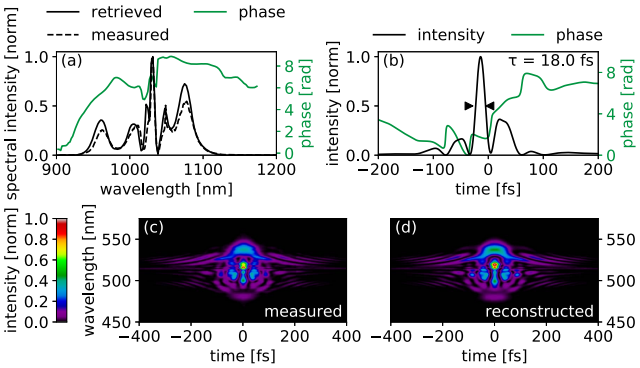

Fig. 3. Temporal characterization after the 3rd stage (965 mbar) at full input power. (a) Spectral intensity and phase, (b) temporal intensity and phase, (c) measured SHG-FROG trace, and (d) reconstructed FROG trace with 0.006 error on a 512 × 512 grid.

Group Delay Dispersion (GDD) and −260 fs^3 Third-Order Dispersion. This ensures an approximately constant pulse duration and peak power over all passes and therefore a constant φ, designed to be about 0.6. All coatings are manufactured in-house. To optimize the flatness of the dispersion curve, the coating is realized as a complementary mirror pair. The first prebroadening stage uses Ø 25.4 mm dispersive mirrors with 300 mm ROC and a mirror separation of 560 mm, allowing 12 passes through two 6.35 mm thick FS windows. Subsequent chirped mirrors introduce −2400 fs^2 GDD by six bounces off the −400 fs^2 GDD mirrors and compress the output to 84 fs. Thus, a SB and compression factor of 2.5 [Fig. 4(a), solid blue line] and a doubling of the peak power are achieved (Table 1). The pulse energy after the first compressor is 2.9 μJ showing 82% efficiency. A second prebroadening stage, using the same mirror spacing and ROC, shortens the pulse further to 43 fs with its chirped-mirror compressor while keeping the pulse energy above 2.6 μJ with an overall efficiency of 74% [Fig. 4(a), solid yellow line]. Here the chirped-mirror compressor consists of four reflections on the −400 fs^2 GDD mirrors. A single 6.35 mm thick FS window is used in the second stage to keep φ below 0.6 as the peak-power is now doubled compared to the first stage. Geometric equality, i.e., the same mode-matching conditions, enables imaging between the first and second stage

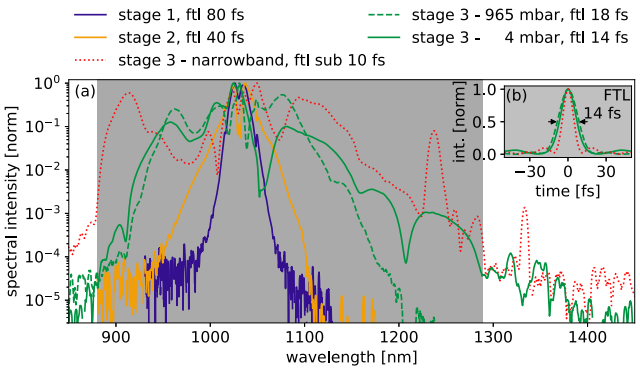

Fig. 4. (a) Spectra in the setup at maximum input power. The curves are measured by an optical spectrum analyzer (Yokogawa). The third stage was measured under ≈965 mbar or 4 mbar of pressure. (b) FTL after the 3rd stage, only power in the shaded area is considered.

which reduces the system's complexity. The third stage comprises two Ø 50.8 mm, 500 mm ROC concave mirrors with the same coating as the first two stages, separated by 894 mm. Mode-matching by two concave mirrors and a beam expander is necessary because the geometries of the second and third HC differ. Thirty-eight passes through a 6.35 mm AR-coated FS window are realized in the third stage, after which the output spectrum's Fourier transform limit (FTL) reaches 18 fs with 2.1 μJ of pulse energy [Figs. 4(a) and 4(b), dashed green line]. 18 fs pulse duration is achieved with a chirped-mirror compressor after the third stage under 965 mbar ambient pressure (Table 1, air). The temporal pulse shape is not optimal [Fig. 3(b)] because only 45% of the pulse energy resides in the main peak, providing 50 MW peak power. One reason for this can be suboptimal dispersion management exhibiting strong overall GDD fluctuations mainly after the dispersive cell mirrors. This statement requires more careful experimental evaluation because the GDD fluctuations might average out over many reflections. Compression close to the FTL would yield a peak power of about 98 MW. The third stage was designed to be optionally operational at 4 mbar ambient pressure where a spectrum supporting a 14 fs FTL can be achieved [Figs. 4(a) and 4(b), dashed green line, Table 1, vac]. The improved SB at reduced pressure is attributed to the elimination of air dispersion, which is estimated to be 550 fs^2 over the 34 m long beam path in the third stage. No further optimization of the pulse compressibility were implemented due to the need to commission this system for further mid-infrared generation experiments. However, previously we showed [28] that tailored dispersive mirrors can successfully compress pulses with a similar non-negligible phase jump around the central wavelength [Fig. 3(a)]. For some applications, e.g., intrapulse difference frequency generation [29], this imperfect compression is not vital. Additionally, to the above-mentioned SB and compression efforts, another experiment was performed by introducing relatively narrowband dispersive cell mirrors in the third compression stage. Surprisingly, it results in even broader bandwidth [Fig. 4(a), red dotted line] with two pronounced peaks near 900 and 1250 nm and can support sub-10 fs FTL pulses. The dispersive mirrors implemented exhibit a strong change of GDD (higher order dispersion) at those wavelengths. Thus, those peaks might be associated with dispersive waves similar to those observed during the SB in solid-core fibers in the presence of strong third-order dispersion [30]. Although not verified, the narrowband mirrors could show improved dispersion compensation by better matching the FS dispersion, explaining the overall increased bandwidth. Yet, the goal of two-cycle pulses necessitates further studies on the compressibility of this spectrum and the mechanism of its large spectral coverage. The beam profiles after the third stage at low power [Fig. 5(d)], at full power [Fig. 5(c)], as well as in the Ø300 μm focus of a 300 mm convex lens [Fig. 5(e)] are compared for the 14 fs FTL case at 4 mbar [Fig. 4(a), green dashed line]. Because of the absence of a characteristic ring pattern, as observed in [12], it is evident that there is negligible influence from nonlinear spatial effects on the beam profile in all cases, which indicates nonlinear phase-shifts per pass below the critical value. This is supported by the good beam focusability implied by the well-behaved beam waist used for further nonlinear experiments. The M^2 factor, measured in accordance with ISO 11670, is below 1.2 in the entire input power range [Fig. 5(b)]. The long-term average power and pointing stability were recorded over 1 h in compliance with the ISO 11670 standard. The output power's normalized root-mean-square (RMS)

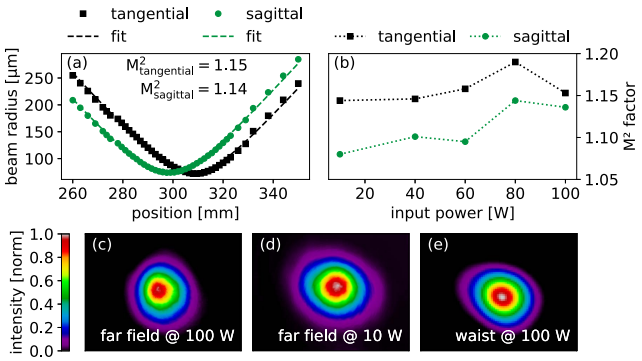

Fig. 5. Beam quality measurement of the 3rd stage (4 mbar): (a) M^2 measurements according to ISO 11146 Performed with Ophir M^2-200-FW-SCOR device. (b) M^2 factor versus input power. (c) Far field beam profile measured at full power. (d) Far field beam profile driven at low power. (e) Attenuated beam profile at a focus at full power (the Si-based beam profiler used is only sensitive in the range 266–1100 nm).

deviation of 0.3% at 50.7 W average power is comparable to the laser source stability of 0.1% (sampled at 10 Hz). It is worth noting that the total path length through the three HC stages amounts to about 50 m. By measuring the centroid location in the focal plane of a ROC 900 mm mirror, the angular beam stability was determined. Over 1 h the RMS in the tangential plane is 43 µrad. In the last 20 min, after thermalization, the RMS is below 10 µrad on both axes. This value compares well to typical thin-disk laser RMS angular stability of 5 µrad [31]. This result was achieved without active beam stabilization and is comparable to commercial lasers [32].

In summary, we demonstrated an efficient spectral-broadening setup, with an output spectrum supporting Fourier-transform limited pulses down to 10 fs. Pulse compression down to 18 fs is experimentally verified. A spectral broadening factor of 22 is achieved by implementing three Herriott-cells with fused silica plates inside. The high-power throughput of 60%, its robustness and simplicity make it an attractive alternative to fiber-based broadening approaches. Further, spectral broadening and compression down to two-optical cycles (7 fs) as well as power scaling experiments, targeting parameters currently available from state-of-the-art fiber systems [33,34], are in progress. The main challenge in this direction is the dispersion compensation over such a large spectral bandwidth in combination with low linear losses. The experiment presented here paves the way towards a compact, all-solid state, amplification-free, oscillator-based XUV source.

Funding. Munich-Centre for Advanced Photonics (MAP); Centre for Advanced Laser Applications (CALA).

Acknowledgment. We thank Dr. K. Mak for his insightful remarks and detailed revision of our work as well as Prof. F. Krausz for the strong support of this research.

REFERENCES

1. M. Herrmann, M. Haas, U. D. Jentschura, F. Kottmann, D. Leibfried, G. Saathoff, C. Gohle, A. Ozawa, V. Batteiger, and S. Knünz, Phys. Rev. A **79**, 052505 (2009).
2. L. von der Wense, B. Seiferle, M. Laatiaoui, J. B. Neumayr, H.-J. Maier, H.-F. Wirth, C. Mokry, J. Runke, K. Eberhardt, and C. E. Düllmann, Nature **533**, 47 (2016).
3. S. Hädrich, J. Rothhardt, M. Krebs, S. Demmler, A. Klenke, A. Tünnermann, and J. Limpert, J. Phys. B **49**, 172002 (2016).
4. C. Heyl, C. Arnold, A. Couairon, and A. L'Huillier, J. Phys. B **50**, 013001 (2016).
5. C. Benko, T. K. Allison, A. Cingöz, L. Hua, F. Labaye, D. C. Yost, and J. Ye, Nat. Photonics **8**, 530 (2014).
6. M. Wunram, P. Storz, D. Brida, and A. Leitenstorfer, Opt. Lett. **40**, 823 (2015).
7. M. Huber, W. Schweinberger, F. Stutzki, J. Limpert, I. Pupeza, and O. Pronin, Opt. Express **25**, 22499 (2017).
8. K. Mak, M. Seidel, O. Pronin, M. Frosz, A. Abdolvand, V. Pervak, A. Apolonski, F. Krausz, J. Travers, and P. S. J. Russell, Opt. Lett. **40**, 1238 (2015).
9. J. Brons, V. Pervak, D. Bauer, D. Sutter, O. Pronin, and F. Krausz, Opt. Lett. **41**, 3567 (2016).
10. C.-H. Lu, Y.-J. Tsou, H.-Y. Chen, B.-H. Chen, Y.-C. Cheng, S.-D. Yang, M.-C. Chen, C.-C. Hsu, and A. H. Kung, Optica **1**, 400 (2014).
11. M. Seidel, J. Brons, G. Arisholm, K. Fritsch, V. Pervak, and O. Pronin, Sci. Rep. **7**, 1410 (2017).
12. M. Seidel, G. Arisholm, J. Brons, V. Pervak, and O. Pronin, Opt. Express **24**, 9412 (2016).
13. B. Zhou, A. Chong, F. Wise, and M. Bache, Phys. Rev. Lett. **109**, 043902 (2012).
14. M. Ueffing, S. Reiger, M. Kaumanns, V. Pervak, M. Trubetskov, T. Nubbemeyer, and F. Krausz, Opt. Lett. **43**, 2070 (2018).
15. L. Lavenu, M. Natile, F. Guichard, Y. Zaouter, X. Delen, M. Hanna, E. Mottay, and P. Georges, Opt. Lett. **43**, 2252 (2018).
16. J. Schulte, T. Sartorius, J. Weitenberg, A. Vernaleken, and P. Russbueldt, Opt. Lett. **41**, 4511 (2016).
17. J. Weitenberg, A. Vernaleken, J. Schulte, A. Ozawa, T. Sartorius, V. Pervak, H.-D. Hoffmann, T. Udem, P. Russbüldt, and T. W. Hänsch, Opt. Express **25**, 20502 (2017).
18. J. Weitenberg, T. Saule, J. Schulte, and P. Rußbüldt, IEEE J. Quantum Electron. **53**, 1 (2017).
19. C. Rolland and P. B. Corkum, J. Opt. Soc. Am. B **5**, 641 (1988).
20. N. V. Sergei, E. V. Koposova, and V. E. Yashin, Quantum Electron. **42**, 989 (2012).
21. A. Weiner, *Ultrafast Optics* (Wiley, 2011), Vol. **72**.
22. J. Brons, "High-power femtosecond laser-oscillators for applications in high-field physics," Ph.D. dissertation (Ludwig Maximilians Universität München, 2017).
23. T. Brabec and F. Krausz, Phys. Rev. Lett. **78**, 3282 (1997).
24. S. C. Pinault and M. J. Potasek, J. Opt. Soc. Am. B **2**, 1318 (1985).
25. D. R. Herriott and H. J. Schulte, Appl. Opt. **4**, 883 (1965).
26. J. U. White, J. Opt. Soc. Am. **32**, 285 (1942).
27. D. Herriott, H. Kogelnik, and R. Kompfner, Appl. Opt. **3**, 523 (1964).
28. O. Pronin, M. Seidel, F. Lücking, J. Brons, E. Fedulova, M. Trubetskov, V. Pervak, A. Apolonski, T. Udem, and F. Krausz, Nat. Commun. **6**, 6988 (2015).
29. I. Pupeza, D. Sánchez, J. Zhang, N. Lilienfein, M. Seidel, N. Karpowicz, T. Paasch-Colberg, I. Znakovskaya, M. Pescher, W. Schweinberger, V. Pervak, E. Fill, O. Pronin, Z. Wei, F. Krausz, A. Apolonski, and J. Biegert, Nat. Photonics **9**, 721 (2015).
30. S. Roy, S. K. Bhadra, and G. P. Agrawal, Phys. Rev. A **79**, 023824 (2009).
31. J. Zhang, J. Brons, N. Lilienfein, E. Fedulova, V. Pervak, D. Bauer, D. Sutter, Z. Wei, A. Apolonski, O. Pronin, and F. Krausz, Opt. Lett. **40**, 1627 (2015).
32. Active Fiber Systems, "Compact 100 w femtosecond laser" (2018). http://www.afs-jena.de/#compact.
33. S. Hadrich, M. Kienel, M. Muller, A. Klenke, J. Rothhardt, R. Klas, T. Gottschall, T. Eidam, A. Drozdy, P. Jojart, Z. Varallyay, E. Cormier, K. Osvay, A. Tunnermann, and J. Limpert, Opt. Lett. **41**, 4332 (2016).
34. H. Carstens, M. Högner, T. Saule, S. Holzberger, N. Lilienfein, A. Guggenmos, C. Jocher, T. Eidam, D. Esser, V. Tosa, V. Pervak, J. Limpert, A. Tünnermann, U. Kleineberg, F. Krausz, and I. Pupeza, Optica **3**, 366 (2016).